Hindawi
Shock and Vibration
Volume 2022, Article ID 3158111, 11 pages
https://doi.org/10.1155/2022/3158111

Research Article

Damage Effects of Shaped Charges on Concrete Piles

Chao-yang Xue, De-ren Kong, and Chun-dong Xu

School of Mechanical Engineering, Nanjing University of Science and Technology, Nanjing 210094, China

Correspondence should be addressed to Chao-yang Xue; xcy0226@njust.edu.cn

Received 16 June 2022; Revised 19 December 2022; Accepted 21 December 2022; Published 29 December 2022

Academic Editor: Ahmed Ibrahim

Concrete piles are a common obstacle in an antilanding obstacle field. To research the damage ability of concrete piles with different shaped charges, penetration tests of concrete piles with different standoff distances (SODs) were carried out with explosively formed projectiles (EFPs) and jetting projectile charges (JPCs). The pressure was measured at different positions inside the concrete piles during the penetration process, and the failure mechanism and damage characteristics of the concrete piles were analyzed. The penetration velocity of the JPC was measured by placing reticular targets inside the concrete pile. The results show that the damage ability of JPCs to concrete piles is stronger than that of EFPs. When the SOD is in the range of 20~50 cm, an EFP causes slight damage to a concrete pile. With the increase in SOD, the penetration capacity of JPCs increases, but the damage ability of JPCs decreases. When the SOD is 15 cm, a JPC causes severe damage to a concrete pile, and when the SOD is in the range of 20~40 cm, a JPC causes moderate damage. When attacking targets with obvious side boundary effects, such as concrete piles, the SOD that results in the strongest damage is not the SOD that results in the strongest penetration ability.

1. Introduction

Concrete is a material widely used in various protection projects [1]. Concrete piles and concrete piles with tracks are common obstacles in antilanding obstacle systems. Breaking down these obstacles is an important task of landing operations.

Thanks to the advantages of high energy utilization and high penetration capability, the shaped charge can destroy concrete targets efficiently. Conducting research work on shaped charge striking concrete targets is of guidance for the design of shaped charges and optimization of concrete structures.

Under the theme of shaped charge penetrating concrete, some scholars have done research work in shaped charges. Wang et al. [2] investigated the effect of liner material on the penetration ability of the shaped charge by conducting concrete penetration tests using three liner materials. Xu et al. [3] designed a bore-centered annular shaped charge (BCASC) and conducted penetration tests on concrete by this shaped charge to investigate the effect of key parameters of this structure on its penetration capability. Zu et al. [4] investigated the particle flow fragmentation process of a Zr-based amorphous alloy. Unlike conventional liner materials, the jet formed by this alloy consists of discrete particles that have the characteristic of not shrinking due to the velocity difference between the head and the tail.

Some scholars have also conducted related research in concrete targets. Esteban et al. [5] and Zhu et al. [6, 7] both performed penetration tests of shaped charge jets on normal strength concrete and ultrahigh strength concrete. The conclusions of both research teams indicate that the penetration ability of the shaped charge into the concrete is not sensitive to the increase in concrete strength level. Xiao et al. [8] conducted penetration tests on reactive powder concrete targets using shaped charges. The results show that the crater diameter of reactive powder concrete under the action of shaped charge penetration is smaller than that of normal strength concrete. Wu et al. [9] conducted shaped charge jet penetration tests on high-strength concrete targets, 45# steel, and high-strength concrete/45# steel composite targets. The results show that different target plate materials have different optimal SODs and the high-strength concrete/45# steel composite target is better than the other two targets.

Most scholars usually choose concrete targets with side hoops surrounded by steel plates or concrete targets with larger radial dimensions when conducting research work related to concrete targets penetrated by shaped charges. These target plates are chosen to reduce the effect of lateral boundary effects on the penetration [10]. Figure 1 shows a structural drawing for the concrete targets covered in the abovementioned literature. The concrete piles used in the landing barrier system have small radial dimensions and do not have steel plate hoops. The influence of the lateral boundaries of this concrete structure on the penetrating action of the shaped charge cannot be ignored.

The dynamic mechanical response of concrete during the penetration process helps to analyze the damage mechanism of concrete. Several scholars have measured the stresses inside concrete under blast loading using PVDF (polyvinylidene fluoride) stress sensors [11, 12]. In addition, some scholars have tested the impact velocity of the projectile on the target [13], but few have measured the penetration velocity of the projectile in the concrete. In summary, there are many studies on shaped charges penetrating concrete targets at this stage. However, in terms of research objects, the concrete targets involved in these studies are relatively single, rarely involving small-sized and nonradially constrained concrete targets; in terms of research methods, few have measured the concrete stresses during the penetration process and almost no one has measured the penetration velocity of the projectile in the concrete targets, thus lacking the discussion and analysis related to stresses and penetration velocities during the penetration process. In order to investigate the destructive ability of different structured shaped charges on small-sized, nonradially restrained concrete targets, this paper conducted penetration tests on concrete piles using EFP and JPC at different SODs. A method of installing stress sensors in concrete was designed to measure the stresses at different locations inside the concrete pile during EFP penetration. A velocity test module was created to measure the penetration velocity of JPC in concrete piles. The damage mechanism and damage characteristics of concrete piles are discussed with the test results of concrete stress and penetration velocity under different SODs. The conclusions drawn can provide a reference for attacking concrete targets with small radial dimensions.

2. Penetration Test

2.1. Shaped Charge. The EFP and JPC were formed using different geometries and angles of the liner. The main charge of the EFP and JPC was JH-2 explosive, which uses a stern structure. The material of the liner was red copper. For the EFP, the structure of the liner was hemispherical with a variable wall thickness. For the JPC, the structure of the liner was an arc-cone bonding structure with a variable wall thickness. The arc-cone bonding part was smooth. The caliber and dimension of the two shaped charges were similar. The structure of the shaped charge is shown in Figure 2. For security reasons, the size and weight of the shaped charge are not disclosed.

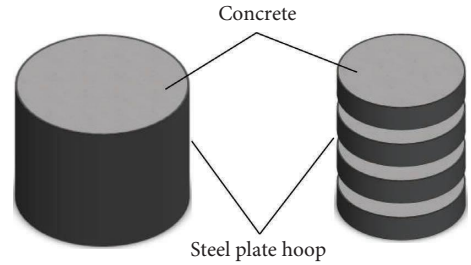

Figure 1: Structural drawing of a common concrete target.

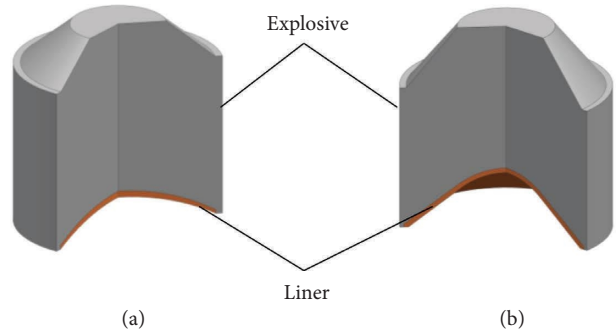

Figure 2: Structure of the shaped charge. (a) EFP. (b) JPC.

2.2. Structure of the Concrete Pile and Layout of Sensors. The C35 concrete pile used in the test is shown in Figure 3. The pile was a regular pyramid structure, with a bottom side length of 1 m, a top side length of 0.6 m, and a height of 0.8 m. After pouring, the concrete pile was naturally preserved for 28 days and then placed in the open air for more than a week. Finally, the test was carried out.

To test the internal stress of concrete piles during penetration, stress sensors were arranged in some concrete piles. The PVDF stress sensor shown in Figure 4 was selected, with a diameter of 40 mm and a thickness of 6 mm. The stress sensor was installed in a specific position using the bracket shown in Figure 5. The sensor signal wire was drawn and tightened from the pipe on the bracket, and then, the pipe was sealed with glue to secure the sensor position. The height of the stress sensor is determined by the height of the opening in the bracket. The horizontal relative position of the stress sensor to the bracket is determined by the length of the pipe on the bracket. The positioning pin of the stress sensor bracket was inserted into the opening in the bottom plate of the concrete mold so that the position of the bracket and the position of the stress sensor could be determined through the opening in the bottom plate. This installation method can minimize the additional stress caused by the fixed constraint of the sensor when the stress wave propagates past the measuring point. The upper part of the bracket was held with the concrete mold to ensure that the bracket and test module did not move during the whole pouring and vibrating process.

To test the penetration velocity of the JPC, reticular targets were set in some concrete piles. Several test modules were poured in advance, in the same way as for the concrete piles. The test modules were $150 * 150 * 75\,\text{mm}^3$ cubes.

Reticular targets made of enameled wire were installed on the upper and lower surfaces of the test modules after curing. The wire spacing of the reticular target was 5 mm. The test modules were supported by a bracket composed of round steel, positioning screws, and metal pads. The bracket was positioned through the opening of the concrete mold bottom plate to ensure that the test module was installed on the central axis of the concrete pile. The height of the test module was determined by positioning screws. The upper part of the bracket was held with the concrete mold to ensure that the bracket and test module did not move during the whole pouring and vibrating process. Figure 6(a) shows the test module with the reticular target installed, and Figure 6(b) shows the test module installed on the bracket.

2.3. Setup. Penetration tests of the concrete pile were carried out using the EFP and JPC. All the shaped charges were set above the center of the top surface of the concrete pile. The SOD was controlled by a bracket made of cardboard. The EFP has a lower depth of penetration than the JPC when the main charges are the same and the charges are of similar caliber and size. Therefore, the penetration velocity of EFP is not tested. Two stress sensors were set in the direction of EFP penetration to test the stress inside the concrete pile during the penetration process, and the stress test direction was the concrete axial direction, which is the direction of EFP penetration. Considering the strong penetration ability of JPC, six layers of mesh targets were set in the JPC penetration path to test the penetration speed of JPC. If the JPC directly hits the stress sensor during the infiltration process, it will have a large influence on the penetration results of the JPC and the output data of the stress sensor will be meaningless. Therefore, the stress sensor is not set inside the concrete pile penetrated by the JPC. The sensor settings are shown in Table 1. As a comparison, the concrete piles in condition 1 and condition 6 are plain concrete without any sensors or test modules.

Figure 7 shows the positions of the sensors in the targets under conditions 2~5 and 7~10. The stress sensors were arranged at different depths on the central axis of the target, and the depths of the two stress sensors were 400 mm and 575 mm. The sensitive surface of the sensor was perpendicular to the central axis of the target, and the stress along the axis was collected. The test modules were arranged at different depths on the central axis of the target according to the position shown. Notably, to ensure the same internal structure of the target, the concrete pile corresponding to conditions 2~5 was equipped with the same test module as conditions 7~10.

3. Results and Discussion

3.1. Damage Results of Concrete Piles

3.1.1. Damage Results of the Concrete Pile under EFP Penetration. Figure 8 shows the damage results of the concrete pile under conditions 1~5 (EFP penetration). Condition 1 involved a plain concrete pile without any sensor or bracket inside, and conditions 2~5 involved concrete piles with sensors and bracket inside. In view of Figure 8, EFP failed to penetrate the concrete pile under the abovementioned five conditions. The rest of the concrete piles were stacked in its original position.

The destructive effect of the projectile on the concrete target consists of the destructive effect of the impact and the destructive effect of the shock wave or stress wave [14]. When the projectile impacts the concrete pile, the compressional wave will propagate in the contact side of the projectile and the concrete pile and the compressive stress generated is far beyond the ultimate compressive strength of the concrete pile, leading to the destruction of the concrete in the contact part into powder. When the impact velocity is greater than the sound velocity of the target, the stress wave generated in the target is a shock wave. When the impact velocity is less than the sound velocity of the target, the stress wave generated is a plastic wave or elastic wave [15]. The sound velocity of concrete can be calculated from the following equation:

$$c = \sqrt{\frac{1-\nu}{(1+\nu)(1-2\nu)}\frac{E}{\rho}}, \tag{1}$$

where c is the velocity of sound, ν is Poisson's ratio, E is Young's modulus, and ρ is the density. The calculated sound velocity of C35 concrete is 3803 m/s. Generally, the velocity of EFP is in the range of 1.5~3 km/s [16]. Therefore, the stress wave generated by EFP impact on the pile is an elastic-plastic wave. The elastic-plastic compressional wave propagates forward in the form of a spherical wave in the concrete. In the propagation process, the stress wave decays rapidly due to the diffusion effect of the spherical wave and the dissipative effect of the concrete. At the initial stage of stress wave propagation, the concrete is crushed when the compressive stress exceeds its dynamic compressive strength. As the shear strength and tensile strength of concrete are far less than its compressive strength, with the attenuation of the stress wave, the concrete is subjected to stress greater than its shear strength and cracks form. At the same time, the concrete produces radial cracks under the action of circumferential tensile stress. Due to the radial extrusion during the penetration of the projectile and the extensional wave generated by the reflection of the stress wave on the side surface (free surface) of the target, the concrete in the crushed area scatters around.

When the stress wave propagates to the interface between the concrete pile and soil, the wave impedance of the concrete is greater than that of the soil, so the transmitted wave of the stress wave in the soil is a compressional wave and the reflected wave in the concrete is an extensional wave. After the test, there was no tensile crack in the lower layer of the remaining concrete pile under conditions 1~5, indicating that the maximum instantaneous tensile stress generated by the joint action of the reflected extensional wave and incident compressional wave did not exceed the ultimate tensile strength of the target. The remaining concrete is the fracture zone.

Table 2 shows the residual heights of the concrete piles under conditions 1~5. For the tested concrete piles, when the

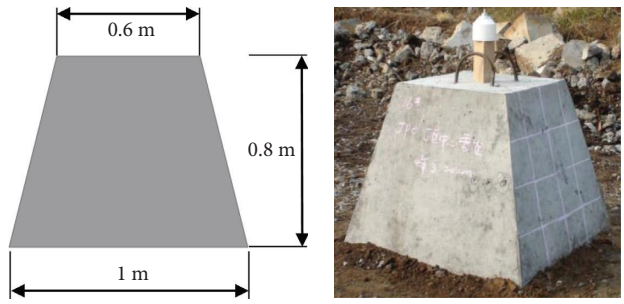

Figure 3: Structure of the concrete pile. (a) Dimensions of concrete piles. (b) Concrete pile.

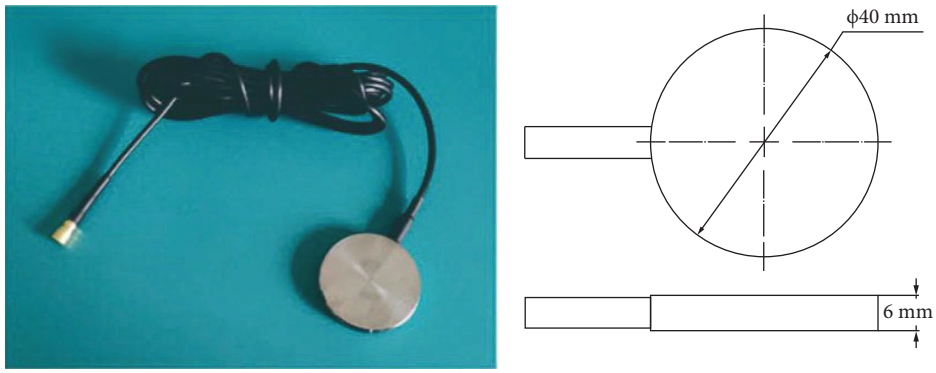

Figure 4: Stress sensor. (a) Physical photo. (b) Specifications of the sensor.

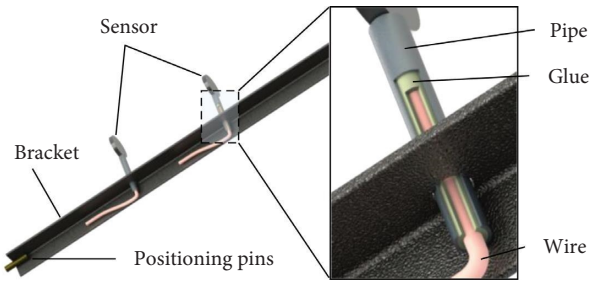

Figure 5: Bracket for the stress sensor.

residual height is higher than 0.5 m, it is judged as slight damage; when the residual height is between 0.4 m and 0.5 m, it is judged as moderate damage, and when the residual height is lower than 0.4 m, it is judged as severe damage. When the SOD is in the range of 20~50 cm, EFP causes slight damage to the concrete pile. Comparing the residual heights of conditions 2~5, it was found that the residual heights of the concrete piles generally show an upward trend with the increase in SOD, but the increase range is small; when the SOD increases from 20 cm to 50 cm, the residual height increases by 5 cm, which accounts for only 6.25% of the concrete pile height, indicating that the damage ability of an EFP to a concrete pile is less affected by the SOD. Comparing the residual heights of condition 1 and condition 3, under the penetration of EFPs with the same SOD, the residual height of the plain concrete pile is 6 cm lower than that of the concrete pile with sensors and bracket inside. This is because the metal bracket improves the tensile strength and shear strength of the concrete pile locally, and the plastic bending deformation of the metal bracket consumes part of the penetration energy, which finally reduces the damage ability of the EFP on the concrete pile.

3.1.2. Damage Results of the Concrete Pile under JPC Penetration. Figure 9 shows the damage results of the concrete pile under conditions 6~10 (JPC penetration). Condition 6 corresponds to a plain concrete pile without any sensor or bracket inside, and conditions 7~10 correspond to concrete piles with sensor bracket inside. In view of Figure 9, in the abovementioned five conditions, the JPC penetrates the concrete pile completely, and the rest of the concrete pile is scattered around.

The penetration process of a JPC is slightly different from that of an EFP. The velocity of JPCs is usually in the range of 3~5 km/s. When a JPC impacts the target, it propagates a shock wave or elastic-plastic wave into the concrete pile. The shock wave propagates to the concrete pile in the form of a spherical wave and gradually decays into an elastic-plastic wave. In the process of JPC penetration, a crushing zone flying around is formed in the upper part of the concrete. JPC penetrates deeper than EFP due to a higher penetration speed and slimmer shape. When JPC penetrates into the lower part of concrete, the lower part of the concrete cannot

(a) (b)

Figure 6: Bracket for the test module. (a) Test module. (b) Bracket.

Table 1: Test conditions.

Charging types	Condition numbers	SOD (cm)	Layout of stress sensors	Number of reticular targets
EFP	1	30	—	0
	2	20	Axial	0
	3	30	Axial	0
	4	40	Axial	0
	5	50	Axial	0
JPC	6	20	—	0
	7	15	—	6
	8	20	—	6
	9	30	—	6
	10	40	—	6

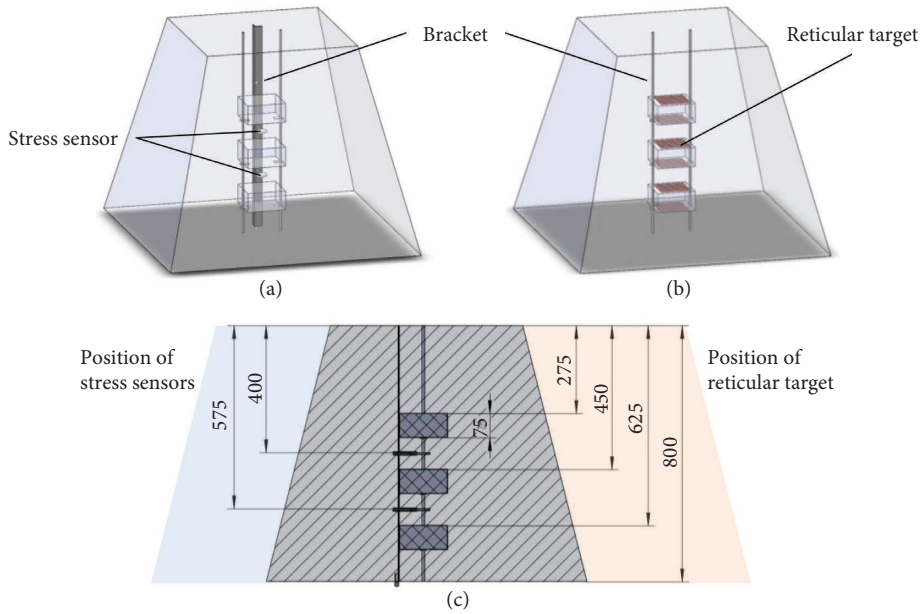

Figure 7: Positions of the sensors. (a) Conditions 2~5. (b) Conditions 7~10. (c) Position dimensions of the sensors.

Figure 8: Damage results of the concrete piles under EFP penetration. (a) Condition 1. (b) Condition 2. (c) Condition 3. (d) Condition 4. (e) Condition 5.

Table 2: Residual height of the concrete pile under EFP penetration.

Condition numbers	1	2	3	4	5
SOD (cm)	30	20	30	40	50
Residual height (cm)	51	54	57	56	59
Damage level	Slight	Slight	Slight	Slight	Slight

become a crushing area completely because the JPC speed decreases gradually and the radial size of concrete increases gradually. According to the spherical cavity expansion theory, when the target is infinite, the projectile impacting the concrete (brittle material) will impact a point at the center of a circle in the concrete and produce a cavity, plastic zone, crack zone, and elastic zone in the radial direction [17, 18]. When JPC penetrates into the lower part of the concrete pile, under the influence of the side boundary, the cavity, plastic zone (crushing zone), and crack zone are successively formed in the radial direction of the concrete. Under the action of JPC reaming extrusion and extensional waves of the free surface, the crack area expands and finally forms damage, as shown in Figure 9.

Table 3 shows the residual height of the concrete pile under conditions 6~10. The residual height here is the maximum height of the concrete fragments. The JPC causes severe damage to the concrete pile with an SOD of 15 cm. When the SOD is in the range of 20~40 cm, the JPC causes moderate damage to the concrete pile. Comparing the

Figure 9: Damage results of the concrete piles under JPC penetration. (a) Condition 6. (b) Condition 7. (c) Condition 8. (d) Condition 9. (e) Condition 10.

residual heights of conditions 7~10, it can be seen that with the increase in the SOD, the residual height of the concrete pile generally increases, and the increase range is large. When the SOD increases from 15 cm to 40 cm, the residual height increases by 11 cm, which accounts for 13.75% of the concrete pile height; this shows that the damage ability of JPCs to concrete piles is greatly affected by the SOD. Comparing the residual heights of condition 6 and condition 8, it can be seen that under the penetration of JPC with the same SOD, the residual height of the plain concrete pile is the same as that of the concrete pile with sensors and brackets inside, indicating that the damage ability of JPCs to concrete piles is less affected by the sensor bracket inside the target.

Comparing the results of Tables 2 and 3 shows that when the SOD is in the range of 20–40 cm, the residual height of the concrete pile under JPC penetration is lower than that under EFP penetration and the former damage level reaches moderate damage, while the latter damage level is only slight.

Table 3: Residual height of the concrete pile under JPC penetration.

Condition numbers	6	7	8	9	10
SOD (cm)	20	15	20	30	40
Residual height (cm)	42	34	42	41	45
Damage level	Moderate	Severe	Moderate	Moderate	Moderate

3.2. Results of the Stress Test. Figure 10 shows stress waveforms at different depths in conditions 3~5. When the SOD is 40 cm, the stress at 400 mm exceeds the sensor range. In

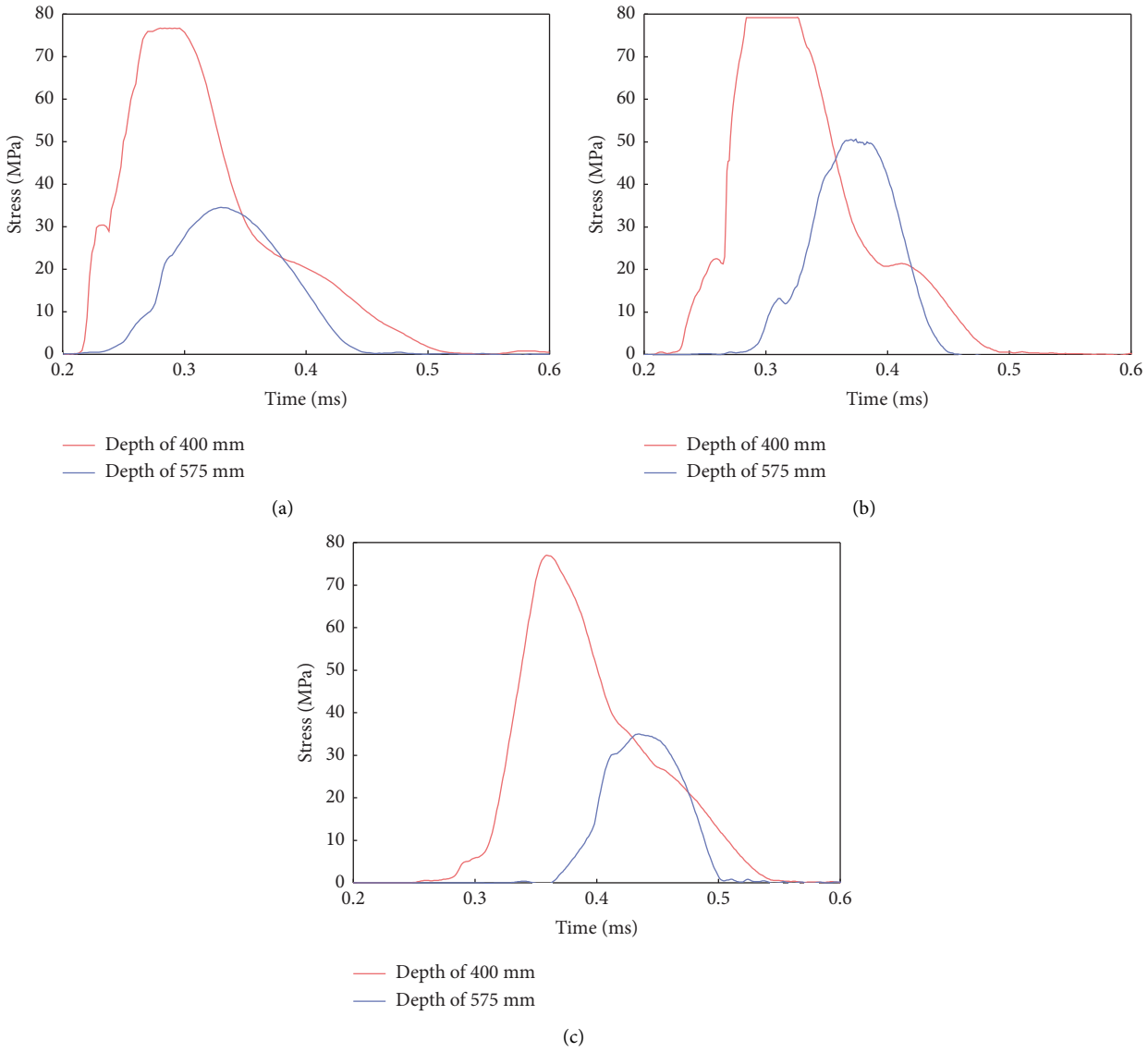

Figure 10: Stress of the concrete pile at different depths during EFP penetration. (a) SOD of 30 cm. (b) SOD of 40 cm. (c) SOD of 50 cm.

view of Figure 10, the peak values of stress waves decrease gradually in the propagation process. A precursor elastic wave can be observed in some of the waveforms, especially in Figure 10(b), where the plastic wave appears after the elastic wave peak. This is because in concrete, the wave velocity of elastic waves is higher than that of plastic waves. By intercepting the signal before the arrival of the plastic wave in Figure 10(b) and using the cross-correlation function to analyze the intercepted signal, the time shift t_s between the two signals was calculated. By dividing the distance of the sensor by t_s, the velocity of the stress wave was calculated to be 3365 m/s. The elastic wave velocity obtained here is smaller than that calculated theoretically above. There are two reasons for this. On the one hand, the actual compressive strength of concrete is lower than 35 MPa. On the other hand, the test module material between the two sensors is poured ten of days in advance (Figure 6(a)). This kind of batch pouring inevitably produces microcracks at the interface of the test module, which become natural defects of the concrete pile. After the testing, it was found that the concrete easily separated at the interface.

Figure 11 shows the stress waveform of the same depth at different SODs. It can be seen from Figure 11 that within the SOD range of 30~50 cm, the peak value of the stress wave at the same measurement point increases first and then decreases with the increase in SOD and the peak value of the stress wave reaches its maximum with the SOD of 40 cm. In view of Figure 11(b), the peak stresses recorded by the lower layer (depth 575 mm) sensor all reached or exceeded the ultimate compressive strength of concrete (35 MPa). For the case of a 40 cm SOD, although the stress waveform shows that the concrete is subjected to greater stress, the remaining height of the concrete pile does not decrease significantly. The greater stress only enlarges the crushed area of the concrete, and the crushed concrete blocks are still piled on the remaining concrete pile. These findings, combined with the results in

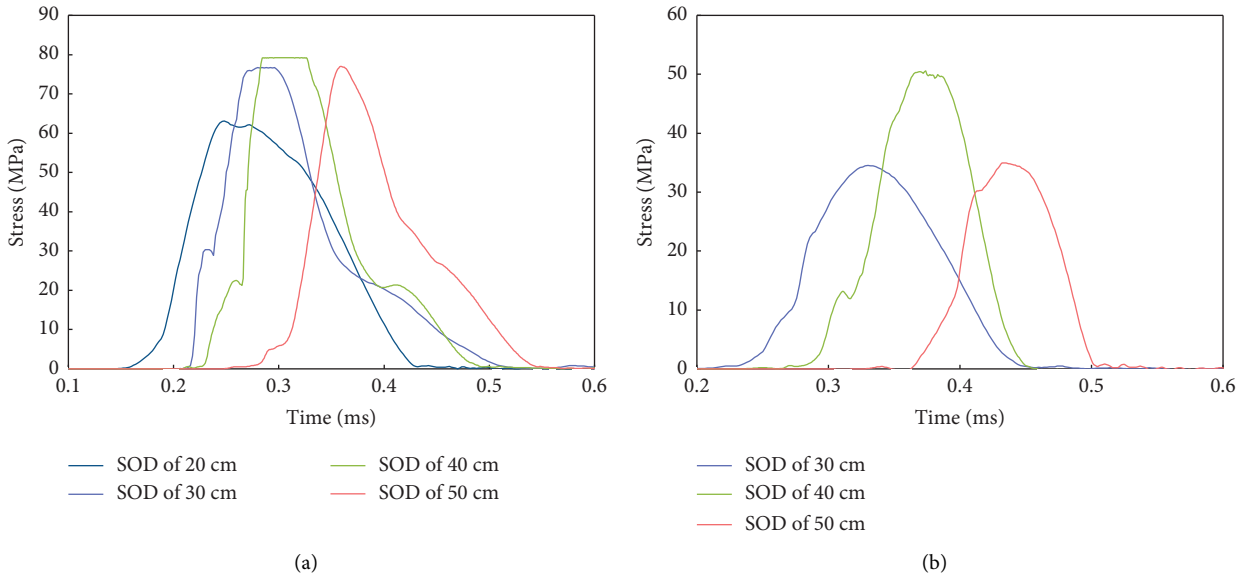

Figure 11: Stress of the concrete pile during EFP penetration with different SODs. (a) Depth of 400 mm. (b) Depth of 575 mm.

Figure 8 and Table 2 mentioned above, show that the residual height of the concrete pile does not decrease significantly with increasing peak axial stress, indicating that the residual height is not highly correlated with the peak stress.

3.3. Results of the Speed Test. Commonly used velocity targets (comb targets and aluminum foil targets) will layer concrete so that the tensile strength and shear strength of concrete at the layered position will be reduced in the process of penetration. To reduce the influence of the velocity target on the concrete strength, a reticular target is used to test the penetration velocity. When the projectile acts on the reticular target at t_0, the reticular target is disconnected, but the projectile may still make the reticular target circuit in the on state. At a later time t_+, when the projectile cannot conduct a current, the test system collects a break signal. In this way, the breaking time of each reticular target collected is actually the t_+ time after the reticular target is broken, and the size of each t_+ may be different. Therefore, the arrival time of the projectile obtained by the test is not sufficiently accurate. However, such imprecision exists for all reticular targets in all conditions, so the test results can still reflect the difference in penetration velocity under different conditions to a certain extent.

Dividing the distance between the two reticular targets by the difference in their disconnection times gives the average penetration velocity between the two reticular targets. This method is used to find the average penetration velocity between each of the two adjacent reticular targets. Figure 12 shows the trend of the average penetration velocity with the penetration depth. The horizontal coordinates of the data points in Figure 12 are taken from the midpoint of each two reticular targets, and the vertical coordinates are the average velocity between the two reticular targets. For the condition with an SOD of 15 cm, the last average velocity is missing because no valid data were measured for the last layer of reticular targets.

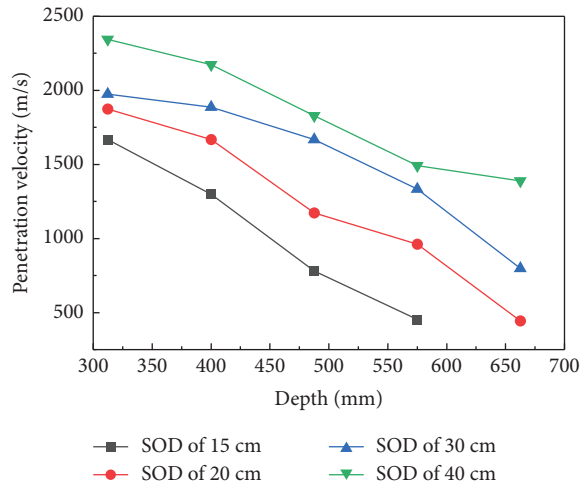

Figure 12: Test results of JPC penetration velocity.

As shown in Figure 12, the penetration speed decreases continuously during the penetration process. When the SOD is in the range of 15~40 cm, the penetration velocity increases with increasing SOD and the penetration velocity between the last two layers of the reticular target increases with increasing SOD, which means that the residual penetration capability increases with increasing SOD. The reason for this trend is that the velocity difference between the head and tail of the JPC leads to continuous elongation during flight. The penetration capability of JPC increases with increasing SOD before it exceeds the optimal SOD. This is consistent with the research results in the literature [19, 20].

Based on the damage results of the concrete piles by JPCs described above, an increasing SOD improves the penetration capacity of JPCs but reduces the damage ability of JPCs to concrete piles. The reason is that the increase in the aspect ratio of the JPC improves its penetration ability but reduces its hole-

expanding ability. For targets with obvious lateral boundary effects, such as concrete piles, the hole-expanding ability of projectiles has a positive effect on enhancing the damage degree. A proper SOD should be selected to avoid wasting energy on redundant penetration capability. The "proper SOD" here is not the "optimal SOD," with the largest penetration depth. For the JPC and concrete piles considered in this research, the "proper SOD" is 15 cm. On the other hand, compared with the damage results of EFP on concrete piles, although EFP has a stronger ability to expand holes than JPC, its damage ability on concrete piles is much worse. In summary, the damage ability of concrete piles by projectiles is jointly determined by their penetration ability and hole-expanding ability, of which the penetration ability plays a major role in the damage degree and the hole-expanding ability affects the damage degree to a certain extent.

4. Conclusions

In this paper, stress sensors and velocity test modules were installed inside the concrete and then the concrete was subjected to a shaped charge penetration test. The test results were analyzed and discussed in detail. The main conclusions are as follows:

(1) When the EFP and JPC with the same charge diameter and similar charge sizes penetrate into the concrete pile at the top center, the damage ability of the JPC to the concrete pile is obviously stronger than that of the EFP to the concrete pile.

(2) The damage ability of EFPs to concrete piles is less affected by the SOD. When the SOD is in the range of 20 cm to 50 cm, EFPs can cause slight damage to concrete piles.

(3) The damage ability of JPCs to concrete piles is greatly affected by the SOD. In the SOD range of 15 cm to 40 cm, with the increase in SOD, the penetration of JPC into the concrete pile gradually increases, but the damage ability gradually decreases. When the SOD is 15 cm, a JPC can cause severe damage to a concrete pile. When attacking targets with obvious side boundary effects, such as concrete piles, the SOD that results in the strongest damage is not the SOD that results in the deepest penetration depth. The appropriate SOD should be selected according to the specific tactical purpose.

In addition, the concrete piles involved in this paper are plain concrete, and reinforced concrete structures should be considered in future studies.

Data Availability

Data are available upon request from the corresponding author.

Conflicts of Interest

The authors declare that there are no conflicts of interest regarding the publication of this paper.

Acknowledgments

The authors would like to acknowledge Scientific Research Project of Nanjing University of Science and Technology (Grant no. 1204011012040) for providing fund for conducting experiments.

References

[1] C. Gao, X. Kong, Q. Fang, Y. Wang, and Y. Yang, "Numerical investigation on attenuation of stress wave in concrete subjected to explosion," *Explosion and Shock Waves*, vol. 42, no. 12, pp. 68–80, 2022.

[2] C. Wang, W. Xu, and S. C. K. Yuen, "Penetration of shaped charge into layered and spaced concrete targets," *International Journal of Impact Engineering*, vol. 112, pp. 193–206, 2018.

[3] W. Xu, C. Wang, J. Yuan, Z. Zhang, and T. Deng, "Assessment of penetration performance and optimum design of a bore-center annular shaped charge," *Propellants, Explosives, Pyrotechnics*, vol. 44, no. 12, pp. 1628–1639, 2019.

[4] X. Zu, T. Chen, Y. Tan, H. Chen, and Z. Huang, "Formation and penetration properties of a shaped charge with Zr41.2Ti13.8Cu12.5Ni10Be22.5 liner," *Nanomaterials*, vol. 12, no. 22, p. 3947, 2022.

[5] B. Esteban, L.-M. Lenhart, L. Rüdiger, and N. Gebbeken, "An evaluation of shaped charge experiments using concrete components," *International Journal of Protective Structures*, vol. 6, no. 3, pp. 439–455, 2015.

[6] Q. Zhu, Z. Huang, Q. Xiao, X. Zu, and X. Jia, "A semi-empirical study of penetration of shaped charge jet into high and ultra-high strength reactive powder concrete targets," *Proceedings of the Institution of Mechanical Engineers - Part C: Journal of Mechanical Engineering Science*, vol. 235, no. 15, pp. 2679–2691, 2021.

[7] Q. F. Zhu, Z. Huang, Q. Xiao, X. Zu, and X. Jia, "Theoretical and experimental study of shaped charge jet penetration into high and Ultra-high strength concrete targets," *International Journal of Impact Engineering*, vol. 122, pp. 431–438, 2018.

[8] Q. Xiao, Z. Huang, X. Zu, X. Jia, Q. Zhu, and W. Cai, "Shaped charge penetration into high- and ultrahigh-strength Steel–Fiber reactive powder concrete targets," *Defence Technology*, vol. 16, no. 1, pp. 217–224, 2020.

[9] H. Wu, F. Hu, and Q. Fang, "A Comparative Study for the Impact Performance of Shaped Charge JET on UHPC Targets," *Defence Technology*, vol. 15, no. 4, pp. 506–518, 2019.

[10] B. Huang, "Experimental study on jet formation and penetration performance of double-layered reactive liners with K-charge," *Chinese Journal of Energetic Materials Hanneng Cailiao*, vol. 29, no. 2, pp. 149–156, 2021.

[11] Y. Hu, J. Liu, W. Gu, and J. Jin, "Stress-testing method by PVDF gauge and its application in explosive test of porous material," *Explosion and Shock Waves*, vol. 36, no. 05, pp. 655–662, 2016.

[12] W. Wang and X. Li, "Experimental study of propagation law of explosive stress wave under condition of decouple charge," *Rock and Soil Mechanics*, vol. 31, no. 06, pp. 1723–1728, 2010.

[13] C. Liu, X. Zhang, H. Chen, J. Wang, H. Wei, and W. Xiong, "Experimental and theoretical study on steel long-rod projectile penetration into concrete targets with elevated impact velocities," *International Journal of Impact Engineering*, vol. 138, Article ID 103482, 2020.

[14] P. Yan, B. Tan, R. Miao, and M. Du, *Warhead and its Damage Principle*, National Defense Industry Press, Arlington, Virginia, 2020.
[15] Z. Huang and X. Zu, *Terminal Effects*, Science Press, Beijing, China, 2014.
[16] X. Zhou, *Missile Damage Effectiveness Test and Evaluation Technology*, National Defense Industry Press, Arlington, Virginia, 2014.
[17] X. Zhang, *Research on the Effect of Drug-type Cover Material on the Penetration of Shaped Jet into Typical High-strength Concrete*, Nanjing University of Science and Technology, Nanjing, China, 2020.
[18] H. Ren, C. Mu, R. Liu, and X. He, *Penetration Effects of Precision Guided Weapons and Engineering protection*, Science Press, Beijing, China, 2016.
[19] X. Yang, J. Han, and W. Li, "Design Method of Optimum Standoff for Bi-Conical Liner Shaped Charge Warhead," *Transactions of Beijing Institute of Technology*, vol. 35, pp. 139–143, 2015.
[20] X. Zhang and F. Huang, "Effects of standoff on the penetration of WCu-Pseudo-Alloy shaped charges in the air and water," *Transactions of Beijing Institute of Technology*, vol. 31, pp. 262–264, 2011.